Colloids and Surfaces A: Physicochem. Eng. Aspects 499 (2016) 18–23

Contents lists available at ScienceDirect

Colloids and Surfaces A: Physicochemical and Engineering Aspects

journal homepage: www.elsevier.com/locate/colsurfa

Superresolution microscopy of the volume phase transition of pNIPAM microgels

Gaurasundar M. Conley[a], Sofi Nöjd[b], Marco Braibanti[a], Peter Schurtenberger[b], Frank Scheffold[a,*]

[a] Department of Physics, University of Fribourg, Chemin du Musée 3, 1700 Fribourg, Switzerland
[b] Physical Chemistry, Department of Chemistry, Lund University, 221 00 Lund, Sweden

HIGHLIGHTS

- Superresolution microscopy applied to study the structure of microgel colloids.
- Microgel radial density profiles revealed in real space.
- Work set's the stage for the use of superresolution microscopy in materials research.
- dSTORM may allow for nanoscale characterization of distinct polymeric subunits in 3D.

GRAPHICAL ABSTRACT

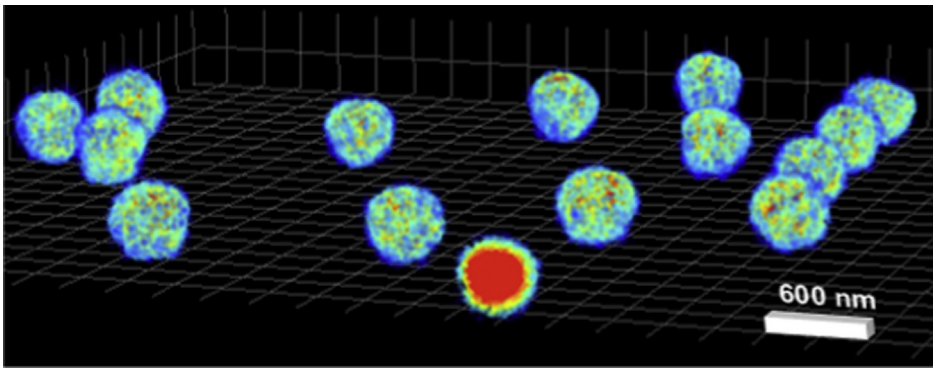

ARTICLE INFO

Article history:
Received 19 January 2016
Received in revised form 3 March 2016
Accepted 4 March 2016
Available online 22 March 2016

Keywords:
Super resolution microscopy
dSTORM
Microgels
pNIPAM

ABSTRACT

Hierarchical polymer structures such as pNIPAM microgels have been extensively studied for their ability to undergo structural and physical transformations that can be controlled by external stimuli such as temperature, pH or solvent composition. However, a direct three-dimensional visualization of individual particles in-situ has so far been hindered by insufficient resolution, with optical microscopy, or contrast, with electron microscopy. In recent years superresolution microscopy techniques have emerged that can provide nanoscopic optical resolution. Here we report on the in-situ superresolution microscopy of dye-labelled submicron sized pNIPAM microgels revealing the internal density profile during swelling and collapse of individual particles. Using direct STochastic Optical Reconstruction Microscopy (dSTORM) we demonstrate a lateral optical resolution of 30 nm and an axial resolution of 60 nm.

1. Introduction

Polymer microgels are a hybrid between a colloid and a polymer and the combination of these two classes of materials offers a number of advantages [1]. The well-defined shape and size of a colloid provides control over the microstructural length scales and response times while the polymeric nature offers physico-chemical control parameters that can be sensitive to external stimuli. The most widely studied material of this kind is based on the polymer poly(N-isopropylacrylamide) (pNIPAM) [1]. It can be cross-linked during synthesis to obtain microgel particles with a size that can be controlled in the range 100–1000 nm. The vast interest stems from

* Corresponding author.
E-mail address: Frank.Scheffold@unifr.ch (F. Scheffold).

http://dx.doi.org/10.1016/j.colsurfa.2016.03.010

the fact that the polymer is thermosensitive with a lower-critical solution temperature of approximately 32 °C in water [2], which is close to physiological conditions. The volume phase transition of the microgels can also be induced by addition of alcohols [3,4] and by changes in pH which offers a plethora of possibilities for the design of stimuli responsive materials and for sensing and substance release applications [5–12]. It has also been argued that the polymer collapse is reminiscent of the protein folding mechanism [13–15]. Despite the overwhelming interest a direct visualization of the volume phase transition of individual particles in-situ has so far been lacking.

The size of microgel particles is typically a micrometre or less and therefore conventional light microscopy cannot resolve its internal structure. Transmission electron microscopy (TEM) is normally only applied to dried and collapsed microgels [16]. In one study cryo-TEM has been applied to swollen polystyrene-pNIPAM core–shell particles at a single temperature [17]. This method, although cumbersome and suffering from low contrast, might have potential for the characterization of the internal density profile of pNIPAM microgels. Equally modern synchroton based X-ray nanotomography, with a resolution in the 50 nm range, could in principle be used [18]. Scattering methods using X-ray, neutrons and light do have the required resolving power and have thus been employed frequently [7,19,20]. However they only provide information about radially averaged properties of an ensemble of particles and thus information on a single part level is not accessible.

In recent years superresolution microscopy techniques have emerged that in principle can provide nanoscopic optical resolution [21–28]. Despite their overwhelming popularity in the field of bioimaging relatively few successful examples for their application in materials sciences are known [29–31]. Here we report on the in-situ superresolution microscopy of pNIPAM microgels revealing the internal density profile during swelling and collapse of individual particles induced by addition of controlled amounts of methanol to the solvent [19].

2. Experimental

2.1. Microgel synthesis and labelling

The microgels are synthesized by free radical precipitation polymerization in a batch reactor using N-isopropylacrylamide (Acros Organics, 99%), NIPAM, as the monomeric unit and N-(3-aminopropyl)methacrylamide hydrochloride (Polysciences), APMA, as a co-monomer. The co-monomer is used in order to incorporate free amine groups into the microgels that are further used as conjugation points for the fluorescent biomarker Alexa Fluor 647. N,N′-Methylenebis(acrylamide) (Sigma–Aldrich, 99%), BIS, is used as a cross-linker. NIPAM is re-crystalized in hexane and all other chemicals are used as received. NIPAM (1.460 g) and BIS (0.103 g) are dissolved in 85 g of H_2O. APMA (0.0066 g) is dissolved in 10 g of H_2O. 5 g of the APMA solution is added to the reactor and the reaction mixture is left to de-gas under an argon atmosphere for 40 min before the temperature is raised to 70 °C. The initiator, 2,2′-Azobis(2-methylpropionamidine) dihydrochloride (Sigma–Aldrich, 97%, 0.0365 g) is dissolved in 5 g of H_2O prior to addition to the reaction mixture. In order to obtain a constant ratio between NIPAM monomers and the co-monomer we continuously add APMA at a constant rate throughout the synthesis following a similar procedure suggested recently by Still and coworkers [32]. Three minutes after the initiator is added the injection pump is started, injecting the remaining 5 g of APMA solution at an addition rate of 0.5 ml/min. The reaction mixture is kept at 70 °C for 4 h before it is left to cool down over night under constant stirring. The suspension is then cleaned by four centrifugation and re-dispersion cycles in order to remove unreacted species. The resulting microgels have a degree of cross-linking of 4.9 mol% and a co-monomer concentration of 0.27 mol% assuming complete consumption of all components. It is known however that the crosslinker BIS is consumed faster than NIPAM which leads to a heterogeneous crosslinking-density in PNIPAM microgels [20]. The continuous addition of the APAM during the synthesis assures that the conjugation points for the fluorophores are distributed homogeneously. To label the microgels we mix them with an excess amount of fluorescent dye Alexa Fluor 647 in water inside a clean Eppendorf vial. We then place it on a slowly oscillating platform at room temperature for 2 h. At least three cycles of centrifugation and resuspension are then performed to remove unreacted dye.

2.2. Sample preparation for dSTORM

Typical experiments last several minutes thus requiring immobilization of the sample. To achieve this we irreversibly adsorb the particles by placing a drop of microgel suspension between two glass coverslips, spreading it into a thin layer, then placing it in the oven at 55 °C until they are dry. The coverslips are previously treated with piranha solution (a mixture of sulfuric acid (H_2SO_4) and hydrogen peroxide (H_2O_2)) to clean them thoroughly. The particles are then resuspended in the appropriate water–methanol solution and found to be immobile for the duration of the experiments. The solution also contains Cysteamine (Sigma–Aldrich) at 50 mM concentration and the pH is adjusted to 8 using HCl. These steps are essential to achieve blinking of fluorophores [28]. In principle, to achieve optimal blinking and therefore the highest possible resolution one should also add oxygen scavengers such as GLOX [28,33] to the imaging solution. We decided to only include cysteamine in order to keep the systems as pure as possible, preserving the microgel deswelling behaviour at the expense of fluorophore brightness and photostability.

2.3. Static and dynamic light scattering

We use a commercial light scattering goniometer (ALV, Germany) for the characterization of the size of the microgel particles in suspension. A green laser wavelength ($\lambda = 532$ nm) is selected because it is only very weakly absorbed by fluorophores present in the microgel structure. We extract the dynamic light scattering hydrodynamic radius R_h from a standard first cumulant fit of the intensity correlation function at three different scattering angles 40°, 50° and 60°. The viscosity of the mixture has been taken from published values [34]. The radius and polydispersity measured by means of static light scattering are obtained by fitting the scattered intensity as a function of the scattering vector q to the fuzzy sphere model [20]. The contribution of back-reflected light at high scattering angles is taken into account with an additional adjustable parameter as described in Ref. [35]. To avoid aggregation of the microgels at higher temperatures we lower the Cysteamine content to 20 mM until the suspension is found stable. To verify that Cysteamine has no influence on particle size we also perform measurements at different concentrations, before the onset of aggregation. We find that size does not depend on the Cysteamine concentration.

2.4. dSTORM superresolution microscopy

We apply direct STochastic Optical Reconstruction Microscopy (dSTORM) for super resolution imaging as described in [28]. To this end we use a 897Nikon TiEclipse inverted microscope, equipped with an EMCCD camera (Andor iXon Ultra) and a total internal reflection fluorescence (TIRF) arm to achieve a highly inclined illumination situation with limited fluorescence background noise. The illumination is provided by a powerful red laser (Coherent

Genesis 1 W at 639 nm) and a weaker violet one (Toptica 120 mW at 405 nm), both coupled into a single mode fibre into the TIRF arm. The light is focused on the back aperture of a high numerical aperture and magnification objective (NA 1.49 and 100× magnification), collimating the beam. Illumination with the red laser is used to achieve sparse fluorophore blinking while the violet laser is used in order to tune the density of blinking molecules. An extra zoom lens is placed before the camera to achieve a final pixel size corresponding to an edge length of 104 nm at the given magnification. A dichroic filter with a central wavelength of 700 nm and bandwidth of 75 nm is placed in the detection pathway (ET700/75, Chroma).

For every image we reconstruct we acquire 60,000 frames with 8–10 ms exposure time and EM gain set to 300. We obtain 3000–5000 fluorophore localizations per particle with typically one to two thousand photons detected per localization. The thousands of images are then analyzed using the open source software ThunderSTORM which determines, for every fluorescent spot, the position, brightness and localization precision [36]. We keep only points that are localized with a precision below 15 nm. To correct for residual small drifts the image stack is subdivided into 20 subsets, each is used to reconstruct an image, then those images are cross correlated to determine drift information. The same software is also used to reconstruct superresolution images [36]. Three-dimensional imaging is performed using the method of astigmatism [21] which we implement using the adaptive optics microscope add-on MicAO (Imagine Optic, France). With the MicAO in place the point spread function changes shape depending on the axial position of the fluorescent emitter. We calibrate for this by imaging fluorescent beads (100 nm diameter, Tetraspeck, Termofisher) scanned through the focal plane. Due to the refractive index mismatch between the sample and the glass a focal shift is present and must be corrected for. As shown in [37], since the sample is within 1.5 μm of the coverslip surface, it is sufficient to rescale allaxial positions by a factor of 0.57 when using the same optics. We determine the nanoscopic resolution from the distribution of measured localizations obtained by the same fluorophore. Although the fluorophore position is immobile it still gives stochastically spread localizations which can be modelled by a Gaussian [21,27]. The full width half maximum (FWHM) then gives us the lateral resolution which we determine to be 30 nm on average. We note that fitting ρ_{2D} for the collapsed microgels with a box profile of constant density equally yields a resolution of ≃30 nm. The axial resolution is estimated to about 60 nm but this value does not enter our quantitative analysis and thus has not been determined with the same accuracy. For comparison the FWHM of the diffraction limited fluorescent spots is approximately 350 nm which means that in our configuration the resolution of the corresponding widefield microscopy is about an order of magnitude lower than dSTORM.

3. Results and discussion

3.1. Light scattering characterization of microgel particles

We prepare dilute pNIPAM microgel particle suspensions at room temperature (T = 22 °C) in a mixture of water and methanol. Pure water is a good solvent for poly(N-isopropylacrylamide) at the selected temperature and the microgels are highly swollen. Methanol is chosen as a deswelling agent because it offers a convenient handle to induce the volume phase transition by changing the solvent composition. Moreover, deswelling with methanol does not require setting accurately different temperatures in the microscope sample chamber. Adding some percentile of methanol induces deswelling until the particles are maximally collapsed for a methanol content of 30% [3,4,38]. We first apply static (SLS)

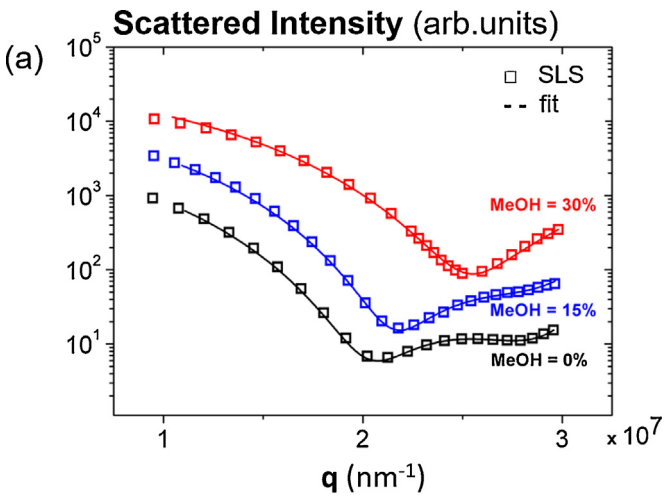

(b)

MeOH (%)	R (nm)	σ_{surf} (nm)	R + 2σ_{surf}	R_h (nm)
0	215	24	263	294
15	205	19	243	250
30	171	1	173	170

Fig. 1. Static and dynamic light scattering characterization of dilute pNIPAM microgel suspensions. (a) Symbols: Static light scattering curves for different methanol contents. Curves are shifted for clarity. Dashed lines: Fit with the fuzzy sphere model for a size polydispersity of 7%. (b) Table of results obtained for the hydrodynamic radius R_h from DLS and R, σ_{surf} extracted from the fit of the SLS data shown in panel (a).

and dynamic light scattering (DLS) to characterize the microgel particles in-situ for different solvent compositions. As we add methanol we observe a shift of the minimum of the scattering curve $I(q)$ towards larger values of q and an increase of the scattered intensity, Fig. 1. These observations show that the microgel particles deswell. We can model the scattering curves quantitatively in the weak scattering or Rayleigh-Gans-Debye approximation considering an isotropic density distribution. To this end we fit the experimental data with the 'fuzzy sphere' model of Stieger et al. [20] taking into account polydispersity and internal reflections in the light scattering cuvette. The model is derived by convoluting the box profile of a homogeneous sphere, radius R, with a Gaussian, standard deviation σ_{surf}. In Fourier space the convolution is represented by a product and the intensity distribution takes the simple form $I(q) \propto \left[3[\sin(qR) - qR\cos(qR)]/\exp(-(\sigma_{surf}q)^2/2)\right]^2$. The simplicity of this expression is to a large extent responsible for the success of this model although it has been recognized early-on that the model is not entirely satisfactory as it does not predict a decay to zero density at a finite distance [1]. Alternative models for the density distribution have been suggested such as an antisymmetric parabolic shell [39], a linear shell profile [40] or a dense core covered by a brush [41,42]. The latter describes well the onset of particle-particle interactions but until now has only been discussed for a brush with constant density [41,43].

In practice we find the fit of the fuzzy sphere model to the light scattering data excellent as shown in Fig. 1. We observe that the particle core radius R shrinks from 215 nm to 171 nm. At the same time the shell of about $2\sigma_{surf} \sim 50$ nm thickness collapses to nearly zero. From dynamic light scattering (DLS) on the same samples we obtain the hydrodynamic radius of the particles R_h. As suggested in previous studies we find that $R + 2\sigma_{surf} \approx R_h$ [20].

3.2. dSTORM imaging of microgel particles

We perform dSTORM [28] measurements by homogeneously illuminating the sample at 639 nm under nearly total internal

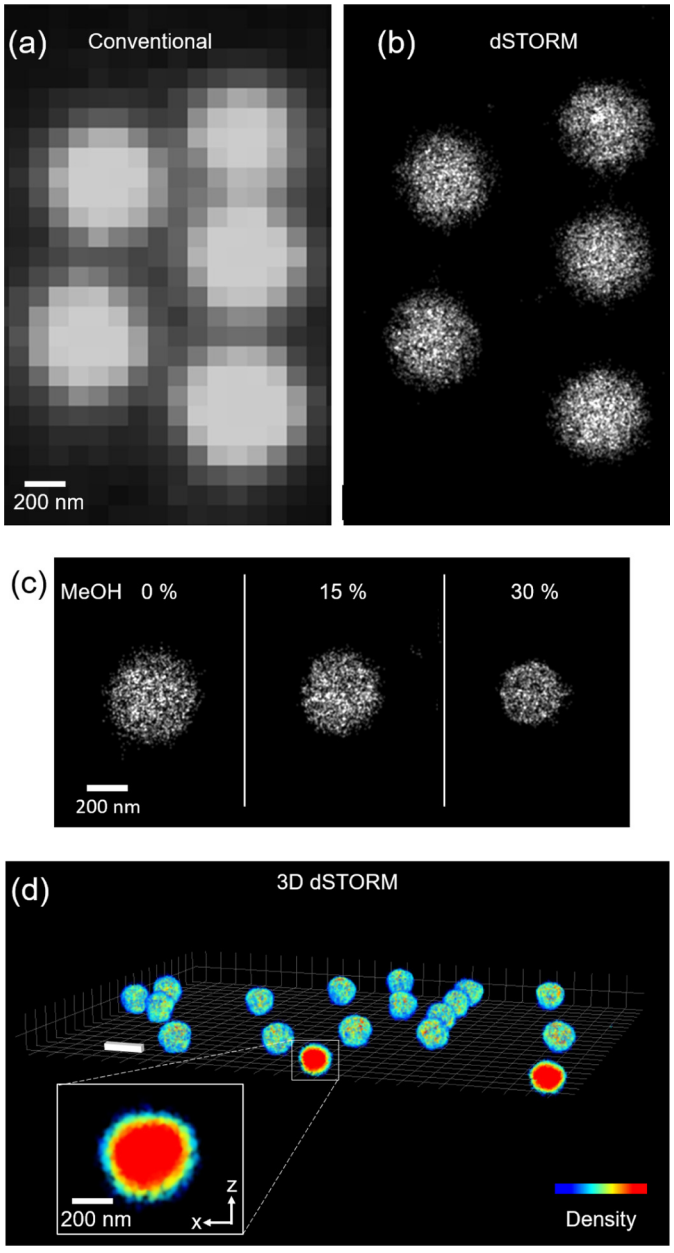

Fig. 2. dSTORM superresolution microscopy of pNIPAM microgels at $T = 22\,^{\circ}C$. (a) Standard widefield fluorescence microscopy image of the swollen microgel particles. (b) dSTORM image of the same sample. (c) dSTORM of the deswelling of the microgel particles upon addition of methanol. (d) 3D image of the swollen microgel particles without the addition of methanol. Grid size is 300 nm, scale bar 600 nm. The inset shows an enlarged view of the density distribution inside an individual particle. dSTORM lateral resolution is ~30 nm and axial resolution is ~60 nm.

reflection conditions. Additional illumination at 405 nm is added when necessary to maintain a sufficient density of blinking fluorophores. In Fig. 2(b) and (c), we show a typical dSTORM images. For comparison we also show an image taken with conventional widefield microscopy under the same conditions in Fig. 2(a). For each dSTORM image we acquire 60,000 frames with an 8–10 ms exposure, resulting in measurement times of 8–10 min. For each frame, images of single fluorophores are fit to 2D Gaussians, determining the x–y position, intensity and localization precision. From this we determine a lateral resolution of 30 nm (FWHM). Several methods are available to obtain three-dimensional superresolution images [21,44–47], out of those we chose that of astigmatism, due to its relative simplicity and availability of software for analysis. With this method the point spread function is distorted in a controlled way, encoding axial position information into its shape. Previous calibration of the distortion allows for the reconstruction of three-dimensional images, as shown in Fig. 2. With this method the axial resolution is lower than in the plane and is estimated to be 60 nm, still an order of magnitude better than confocal microscopy. Such 3D imaging on the nanoscale might not be crucial for more or less isotropic microgels but will become of key importance whenever the particle architecture is more complex such as for ellipsoidal particles or heterogeneous structures [48–50]. In our experiments we do not observe an anisotropy of the particles and we therefore decided to take advantage of the higher lateral resolution for the quantitative analysis of the radial density distribution inside the microgel particle. All density profiles are thus modelled based on the 2D projection of detected sites on the plane of observation.

3.3. Microgel density profiles

In Fig. 3 we show the measured ensemble averaged 2D density profiles $\rho_{2D}(r)$ for three different solvent compositions. Note

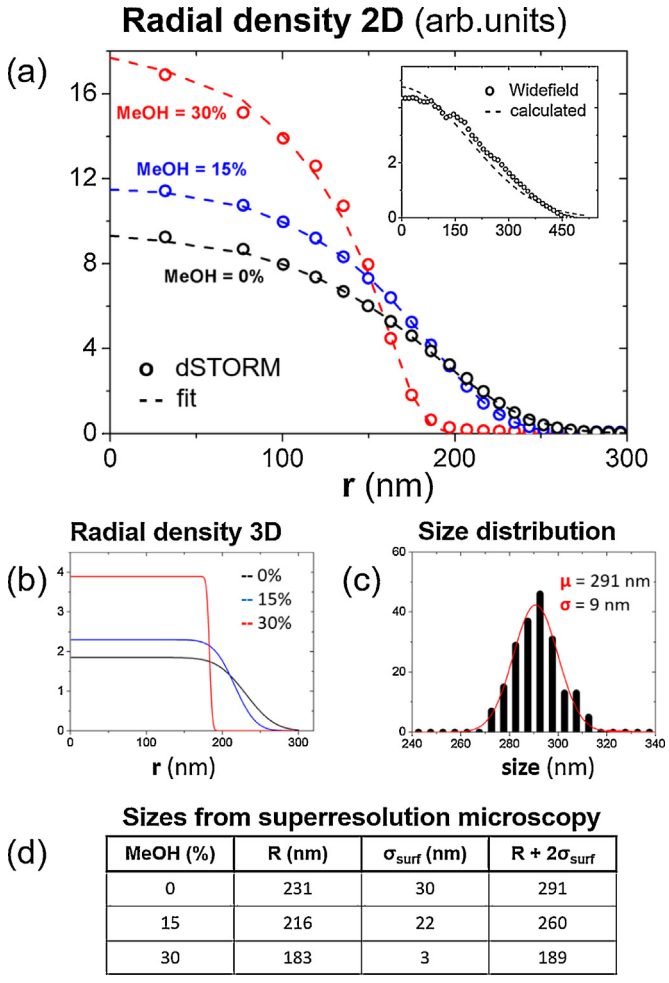

(d) Sizes from superresolution microscopy

MeOH (%)	R (nm)	σ_{surf} (nm)	R + 2σ_{surf}
0	231	30	291
15	216	22	260
30	183	3	189

Fig. 3. dSTORM analysis of the microgel radial density profile. (a) Symbols: Measured 2D density profiles (average over about one hundred particles). Dashed lines: Fit with the fuzzy sphere model with a core radius R, a shell parameter σ_{surf} and a fixed dSTORM resolution of 30 nm (FWHM). Inset: Measured 2D density profile from widefield fluorescence microscopy images of swollen pNIPAM microgels as shown in Fig. 2(a). The dashed line is calculated using $R = 231$ nm, $\sigma_{surf} = 30$ nm taken from Table 1(b) and a resolution of 350 nm (FWHM). (b) 3D radial density profiles corresponding to the fits shown in (a). (c) Distribution of size $R + 2\sigma_{surf}$ obtained from fitting the density profile of individual particles. Average size $\mu = 291$ nm, standard deviation $\sigma = 9$ nm (MeOH = 0%). (d) Table of results for the mean particle core radius and shell determined by dSTORM.

that due to the projection a homogeneous sphere with radius R appears as $\rho_{2D}(r) \propto \sqrt{(R^2 - r^2)}; r \leq R$. Moreover we have to include the finite resolution $\xi \simeq 30$ nm (FWHM) in our analysis. Next we fit images of the swollen microgels while keeping ξ constant. We apply the fuzzy sphere model by Stieger et al. [20] that we had used to model the static light scattering curves, Fig. 1. The adjustable fit parameters are the core radius R and the smearing parameter σ_{surf} which corresponds to about half the thickness of the fuzzy shell. In 3D the model predicts a density distribution $\rho(r) \propto erfc(r - R, \sigma_{surf})$. For the fit we convolute this function to take account for the finite resolution $\xi = 30$ nm, project it to the plane and adjust R, σ_{surf} until we obtain a best fit (see also supporting information). The results are shown in Fig. 3(a) as dashed lines. The core radius and the smearing parameter σ_{surf} extracted from the fit are in quantitative agreement with the scattering results. The corresponding radial density profiles in 3D are shown in Fig. 3(b). For a comparison we also show a measured 2D density profiles obtained from standard widefield microscopy, Fig. 2(a). With a resolution of $\xi \simeq 350$ nm (FWHM) we find this data in agreement with the predictions calculated based on the light scattering results (dashed line). The largely inferior resolution however does not permit a meaningful independent analysis of the radial density profile. In Fig. 3(c), we show the results for the particle size obtained by analysing the density profiles of individual microgels. From this data we can extract the polydispersity (standard deviation divided by the mean) of the particle size $\sim R + 2\sigma_{surf}$ and find a value of 3.1%. This value is somewhat smaller than the one obtained from static light scattering, Fig. 1. We believe this discrepancy is due to the failure of the Rayleigh Gans Debye approximation in light scattering due to the finite refractive index contrast even for the low density swollen microgels [19]. The latter result is a hint for the power of a visualization of the individual microgels: it allows a direct real-space interpretation of the experimental results and thus in many cases can provide more accurate information.

4. Summary and conclusions

In summary we could demonstrate the successful application of dSTORM superresolution microscopy to stimuli-responsive pNIPAM microgels. For the microgels studied the dSTORM results are in quantitative agreement with static and dynamic light scattering. Our results can serve as a benchmark and open the pathway for future applications towards more complex polymer and microgel architectures. Anisotropic, deformed or core–shell microgels as well as microgels that are doped or decorated with metal nanoparticles can be studied [49,50]. Such systems are difficult or impossible to characterize in-situ with conventional techniques. Moreover a generalization of our approach using multicolor dSTORM [51] can be applied in a next step for the nanoscale characterization and colocalization of functional, chemically distinct subunits of colloidal particles.

Acknowledgements

This work was supported by the Swiss National Science Foundation through project number 149867, and through the National Centre of Competence in Research *Bio-Inspired Materials*. We acknowledge financial support by the Adolphe Merkle Foundation. We thank Isabelle Spühler, Georges Brügger, Veronique Trappe and Davide Calzolari for fruitful discussions. PS gratefully acknowledges support from the European Research Council (ERC-339678-COMPASS) and the Swedish Research Council (621-2014-4037).

Appendix A. Supplementary data

Supplementary data associated with this article can be found, in the online version, at http://dx.doi.org/10.1016/j.colsurfa.2016.03.010.

References

[1] A. Fernandez-Nieves, H. Wyss, J. Mattsson, D.A. Weitz, Microgel Suspensions: Fundamentals and Applications, John Wiley & Sons, 2011.
[2] C. Wu, X. Wang, Globule-to-coil transition of a single homopolymer chain in solution, Phys. Rev. Lett. 80 (18) (1998) 4092.
[3] F.M. Winnik, H. Ringsdorf, J. Venzmer, Methanol-water as a co-nonsolvent system for poly(n-isopropylacrylamide), Macromolecules 23 (8) (1990) 2415–2416.
[4] R.O. Costa, R.F. Freitas, Phase behavior of poly(n-isopropylacrylamide) in binary aqueous solutions, Polymer 43 (22) (2002) 5879–5885.
[5] A. Fernandez de las Nieves, H. Wyss, J. Mattson, D.A. Weitz (Eds.), Microgel Suspensions: Fundamentals and Applications, 2011.
[6] M.J. Snowden, B.Z. Chowdhry, B. Vincent, G.E. Morris, Colloidal copolymer microgels of n-isopropylacrylamide and acrylic acid: pH, ionic strength and temperature effects, J. Chem. Soc. Faraday Trans. 92 (24) (1996) 5013–5016.
[7] M. Ballauff, Y. Lu, Smart nanoparticles: preparation, characterization and applications, Polymer 48 (7) (2007) 1815–1823.
[8] I. Berndt, W. Richtering, Doubly temperature sensitive core–shell microgels, Macromolecules 36 (23) (2003) 8780–8785.
[9] M.R. Islam, A. Ahiabu, X. Li, M.J. Serpe, Poly(n-isopropylacrylamide) microgel-based optical devices for sensing and biosensing, Sensors 14 (5) (2014) 8984–8995.
[10] A. Sánchez-Iglesias, M. Grzelczak, B. Rodríguez-González, P. Guardia-Giros, I. Pastoriza-Santos, J. Pérez-Juste, M. Prato, L.M. Liz-Marzán, Synthesis of multifunctional composite microgels via in situ Ni growth on pNIPAM-coated Au nanoparticles, ACS Nano 3 (10) (2009) 3184–3190.
[11] R. Contreras-Cáceres, S. Abalde-Cela, P. Guardia-Girós, A. Fernández-Barbero, J. Pérez-Juste, R.A. Alvarez-Puebla, L.M. Liz-Marzán, Multifunctional microgel magnetic/optical traps for SERS ultradetection, Langmuir 27 (8) (2011) 4520–4525.
[12] C.M. Nolan, M.J. Serpe, L.A. Lyon, Thermally modulated insulin release from microgel thin films, Biomacromolecules 5 (5) (2004) 1940–1946.
[13] C.M. Dobson, A. Fersht, Protein Folding, Cambridge Univ Press, 1996.
[14] G. Graziano, On the temperature-induced coil to globule transition of poly-n-isopropylacrylamide in dilute aqueous solutions, Int. J. Biol. Macromol. 27 (1) (2000) 89–97.
[15] H. Chen, J. Li, Y. Ding, G. Zhang, Q. Zhang, C. Wu, Folding and unfolding of individual pNIPAM-g-PEO copolymer chains in dilute aqueous solutions, Macromolecules 38 (10) (2005) 4403–4408.
[16] C. Dagallier, H. Dietsch, P. Schurtenberger, F. Scheffold, Thermoresponsive hybrid microgel particles with intrinsic optical and magnetic anisotropy, Soft Matter 6 (10) (2010) 2174–2177.
[17] J.J. Crassous, C.N. Rochette, A. Wittemann, M. Schrinner, M. Ballauff, M. Drechsler, Quantitative analysis of polymer colloids by cryo-transmission electron microscopy, Langmuir 25 (14) (2009) 7862–7871.
[18] P.J. Withers, X-ray nanotomography, Mater. Today 10 (12) (2007) 26–34.
[19] M. Reufer, P. Dıaz-Leyva, I. Lynch, F. Scheffold, Temperature-sensitive poly(n-isopropyl-acrylamide) microgel particles: a light scattering study, Eur. Phys. J. E 28 (2) (2009) 165–171.
[20] M. Stieger, W. Richtering, J.S. Pedersen, P. Lindner, Small-angle neutron scattering study of structural changes in temperature sensitive microgel colloids, J. Chem. Phys. 120 (13) (2004) 6197–6206.
[21] B. Huang, W. Wang, M. Bates, X. Zhuang, Three-dimensional super-resolution imaging by stochastic optical reconstruction microscopy, Science 319 (5864) (2008) 810–813.
[22] B. Huang, M. Bates, X. Zhuang, Super resolution fluorescence microscopy, Annu. Rev. Biochem. 78 (2009) 993.
[23] S.W. Hell, Far-field optical nanoscopy, Science 316 (5828) (2007) 1153–1158.
[24] C.G. Galbraith, J.A. Galbraith, Super-resolution microscopy at a glance, J. Cell Sci. 124 (10) (2011) 1607–1611.
[25] E. Betzig, G.H. Patterson, R. Sougrat, O.W. Lindwasser, S. Olenych, J.S. Bonifacino, M.W. Davidson, J. Lippincott-Schwartz, H.F. Hess, Imaging intracellular fluorescent proteins at nanometer resolution, Science 313 (5793) (2006) 1642–1645.
[26] S.W. Hell, Microscopy and its focal switch, Nat. Methods 6 (1) (2009) 24–32.
[27] M. Heilemann, S. van de Linde, M. Schüttpelz, R. Kasper, B. Seefeldt, A. Mukherjee, P. Tinnefeld, M. Sauer, Subdiffraction-resolution fluorescence imaging with conventional fluorescent probes, Angew. Chem. Int. Ed. 47 (33) (2008) 6172–6176.
[28] S. van de Linde, A. Löschberger, T. Klein, M. Heidbreder, S. Wolter, M. Heilemann, M. Sauer, Direct stochastic optical reconstruction microscopy with standard fluorescent probes, Nat. Protoc. 6 (7) (2011) 991–1009.
[29] S. Habuchi, S. Onda, M. Vacha, Molecular weight dependence of emission intensity and emitting sites distribution within single conjugated polymer molecules, Phys. Chem. Chem. Phys. 13 (5) (2011) 1743–1753.

[30] H. Aoki, K. Mori, S. Ito, Conformational analysis of single polymer chains in three dimensions by super-resolution fluorescence microscopy, Soft Matter 8 (16) (2012) 4390–4395.
[31] A.J. Berro, A.J. Berglund, P.T. Carmichael, J.S. Kim, J.A. Liddle, Super-resolution optical measurement of nanoscale photoacid distribution in lithographic materials, ACS Nano 6 (11) (2012) 9496–9502.
[32] T. Still, K. Chen, A.M. Alsayed, K.B. Aptowicz, A. Yodh, Synthesis of micrometer-size poly(n-isopropylacrylamide) microgel particles with homogeneous crosslinker density and diameter control, J. Colloid Interface Sci. 405 (2013) 96–102.
[33] G.T. Dempsey, J.C. Vaughan, K.H. Chen, M. Bates, X. Zhuang, Evaluation of fluorophores for optimal performance in localization-based super-resolution imaging, Nat. Methods 8 (12) (2011) 1027–1036.
[34] D.R. Lide, CRC Handbook of Chemistry and Physics, CRC press, 2004.
[35] T. Zemb, P. Lindner, Neutrons, X-rays and Light: Scattering Methods Applied to Soft Condensed Matter, North-Holland, 2002.
[36] M. Ovesn'y, P. Kří žek, J. Borkovec, Z. Švindrych, G.M. Hagen, ThunderSTORM: a comprehensive ImageJ plug-in for PALM and STORM data analysis and super-resolution imaging, Bioinformatics 30 (16) (2014) 2389–2390.
[37] B.P. Bratton, J.W. Shaevitz, Simple experimental methods for determining the apparent focal shift in a microscope system, PLOS ONE 10 (8) (2015) e0134616.
[38] I. Bischofberger, D. Calzolari, P. De Los Rios, I. Jelezarov, V. Trappe, Hydrophobic hydration of poly-n-isopropyl acrylamide: a matter of the mean energetic state of water, Sci. Rep. (2014) 4, Article number: 4377.
[39] I. Berndt, J.S. Pedersen, W. Richtering, Structure of multiresponsive "intelligent" core–shell microgels, J. Am. Chem. Soc. 127 (26) (2005) 9372–9373.
[40] T. Mason, M. Lin, Density profiles of temperature-sensitive microgel particles, Phys. Rev. E 71 (4) (2005) 040801.
[41] F. Scheffold, P. Díaz-Leyva, M. Reufer, N.B. Braham, I. Lynch, J.L. Harden, Brush-like interactions between thermoresponsive microgel particles, Phys. Rev. Lett. 104 (12) (2010) 128304.
[42] G. Romeo, M.P. Ciamarra, Elasticity of compressed microgel suspensions, Soft Matter 9 (22) (2013) 5401–5406.
[43] J.U. Kim, M.W. Matsen, Compression of polymer brushes: quantitative comparison of self-consistent field theory with experiment, Macromolecules 42 (9) (2009) 3430–3432.
[44] M.F. Juette, T.J. Gould, M.D. Lessard, M.J. Mlodzianoski, B.S. Nagpure, B.T. Bennett, S.T. Hess, J. Bewersdorf, Three-dimensional sub-100 nm resolution fluorescence microscopy of thick samples, Nat. Methods 5 (6) (2008) 527–529.
[45] S.R.P. Pavani, M.A. Thompson, J.S. Biteen, S.J. Lord, N. Liu, R.J. Twieg, R. Piestun, W. Moerner, Three-dimensional, single-molecule fluorescence imaging beyond the diffraction limit by using a double-helix point spread function, Proc. Natl. Acad. Sci. U. S. A. 106 (9) (2009) 2995–2999.
[46] J. Deschamps, M. Mund, J. Ries, 3D superresolution microscopy by supercritical angle detection, Opt. Express 22 (23) (2014) 29081–29091.
[47] G. Shtengel, J.A. Galbraith, C.G. Galbraith, J. Lippincott-Schwartz, J.M. Gillette, S. Manley, R. Sougrat, C.M. Waterman, P. Kanchanawong, M.W. Davidson, et al., Interferometric fluorescent super-resolution microscopy resolves 3D cellular ultrastructure, Proc. Natl. Acad. Sci. U. S. A. 106 (9) (2009) 3125–3130.
[48] M. Karg, I. Pastoriza-Santos, J. Pérez-Juste, T. Hellweg, L.M. Liz-Marzán, Nanorod-coated PNIPAM microgels: thermoresponsive optical properties, Small 3 (7) (2007) 1222–1229.
[49] J.-F. Dechézelles, V. Malik, J.J. Crassous, P. Schurtenberger, Hybrid raspberry microgels with tunable thermoresponsive behavior, Soft Matter 9 (10) (2013) 2798–2802.
[50] J.J. Crassous, A.M. Mihut, L.K. Månsson, P. Schurtenberger, Anisotropic responsive microgels with tuneable shape and interactions, Nanoscale 7 (38) (2015) 15971–15982.
[51] A. Lampe, V. Haucke, S.J. Sigrist, M. Heilemann, J. Schmoranzer, Multi-colour direct storm with red emitting carbocyanines, Biol. Cell 104 (4) (2012) 229–237.